# Magnetic neutron scattering (invited)

J. W. Lynn
*Reactor Radiation Division, National Institute of Standards and Technology, Gaithersburg, Maryland 20899*

The application of neutron scattering techniques to magnetic problems is reviewed. We will first discuss diffraction techniques used to solve magnetic structures, as well as to measure magnetic form factors, order parameters, critical phenomena, and the scattering from low-dimensional systems. We will also discuss inelastic scattering techniques, including polarized beam methods, utilized to determine the spin dynamics of various materials. Information will be provided about the types of spectrometers available at the user-oriented national facilities located at Argonne National Laboratory, Brookhaven National Laboratory, Los Alamos National Laboratory, The National Institute of Standards and Technology, and Oak Ridge National Laboratory, as well as the spectrometers at the Missouri University Research Reactor.

## I. INTRODUCTION

Magnetic neutron scattering plays a central role in determining and understanding the microscopic properties of a vast variety of magnetic systems, from the fundamental nature and symmetry of magnetically ordered materials to elucidating the magnetic characteristics essential in applications. One traditional role has been the measurement of magnetic Bragg intensities in the magnetically ordered regime, which can be used to determine not only the spatial arrangement and atomic magnetization density of the magnetic moments, but also the value of the ordered moments as a function of temperature, pressure, and applied magnetic field. These types of measurements can be carried out on single crystals, powders, thin films, and multilayers, and often the information collected can be obtained by no other experimental technique. Small angle neutron scattering (SANS) is a technique to explore the magnetism over longer distances than conventional diffraction, and is ideal to study domain structures and other spatial variations of the magnetization density on length scales from 1–1000 nm. The relatively new technique of neutron reflectometry can be used to explore the magnetization distribution in the near-surface regime of thin films, multilayers, and crystals. In the investigation of the spin dynamics of systems, though, neutrons play a truly unique role. Neutron scattering is the only technique that can directly determine the complete magnetic excitation spectrum, whether it is in the form of the dispersion relations for spin wave excitations, wave vector and energy dependence of critical fluctuations, crystal field excitations, moment fluctuations, etc. In the present article we will briefly discuss some of these possibilities, and present a few examples taken from recent work at NIST. We will also discuss the neutron instrumentation presently available to the magnetism community, and plans for new instrumentation which will take the field into the next decade and beyond.

There are a number of very good sources of detailed information about neutron scattering. The textbook by Lovesey[1] treats the theory of neutron scattering in depth, and the more recent work of Balcar and Lovesey[2] specifically addresses the theory for the case of magnetic neutron as well as x-ray scattering. Bacon's text[3] is more for the experimentalist, treating experimental procedures and the practicalities of taking and analyzing data. Williams' text[4] focuses on the use of polarized neutrons, while Squires' book[5] is more of a graduate introductory text to the subject. An alternative reference is the recent compendium by Price and Sköld,[6] which covers a variety of topics in neutron scattering in the form of chapters by various experts.

## II. MAGNETIC DIFFRACTION

The integrated intensity for a magnetic Bragg reflection is given (for a simple collinear magnetic structure) by[1]

$$I_M = C\mathscr{M}_\tau A(\theta_B)\left(\frac{\gamma e^2}{2mc^2}\right)^2 \langle 1-(\hat{\tau}\cdot\hat{M})^2\rangle |F_M|^2, \qquad (1)$$

where the neutron-electron coupling constant in parenthesis is $-0.27\times10^{-12}$ cm, $\hat{\tau}$ and $\hat{M}$ are unit vectors in the direction of the reciprocal lattice vector $\boldsymbol{\tau}$ and the spin direction, respectively, and the orientation factor $\langle 1-(\hat{\tau}\cdot\hat{M})^2\rangle$ must be calculated for all possible domains. $C$ is an instrumental constant which includes the resolution of the measurement, $A(\theta_B)$ is an angular factor which depends on the method of measurement, and $\mathscr{M}_\tau$ is the multiplicity of the reflection (for powders). The magnetic structure factor $F_M$ is given by

$$F_M = \sum_{j=1}^{N} \langle \mu_z\rangle_j f_j(\boldsymbol{\tau}) e^{-W_j} e^{i\boldsymbol{\tau}\cdot\mathbf{r}_j}, \qquad (2)$$

where $\langle \mu_z\rangle_j$ is the thermal average of the aligned magnetic moment of the magnetic ion at the $j$th site at position $\mathbf{r}_j$, $W_j$ is the Debye Waller factor for the $j$th atom, $f(\boldsymbol{\tau})$ is the magnetic form factor (Fourier transform of the magnetization density), and the sum extends over all magnetic atoms in the unit cell. We see from these expressions that neutrons can be used to determine several important quantities; the location of magnetic atoms and the spatial distribution of their magnetic electrons; the temperature, field,... dependence of $\langle \mu_z\rangle$, which is directly related to the order parameter for the phase

 0021-8979/94/75(10)/6806/5/$6.00 © 1994 American Institute of Physics

Downloaded 10 Nov 2003 to 129.6.121.15. Redistribution subject to AIP license or copyright, see http://ojps.aip.org/japo/japcr.jsp

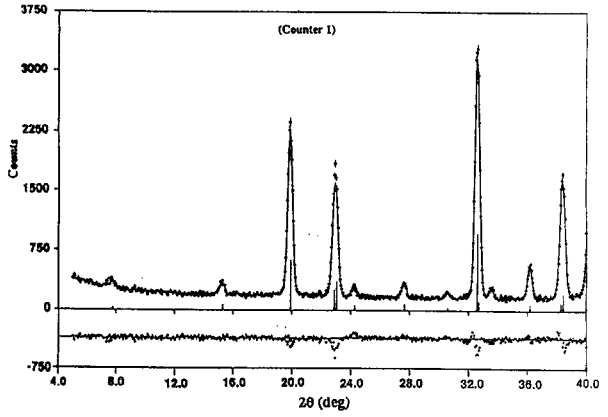


FIG. 1. Calculated (solid curve) and observed intensities for a powder of $YBa_2Fe_3O_8$. The differences between calculated and observed are shown at the bottom (Ref. 7).

transition (e.g., sublattice magnetization). The preferred magnetic axis ($\hat{M}$) also can often be determined from the relative intensities. Finally, the scattering can be put on an absolute scale by internal comparison with the nuclear Bragg intensities from the same sample, whereby the saturated value of the magnetic moment can be obtained.

As an example, a portion of the powder diffraction pattern from a sample of $YBa_2Fe_3O_8$ is shown in Fig. 1.[7] The solid curve is a profile refinement of both the antiferromagnetic and crystallographic structure for the sample. From this type of data we can determine the crystal structure, lattice parameters, site occupancies, etc., as well as the magnetic structure and value of the ordered moment. The results of the analysis are shown in Fig. 2; the crystal structure is identical to the structure for the 1-2-3 superconductor with the Fe replacing the Cu, and the magnetic structure is also the same as has been observed for the Cu spins in the oxygen-reduced (semiconducting) material.

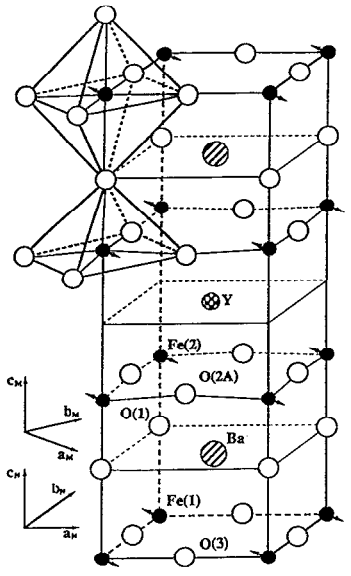


FIG. 2. Crystal and magnetic structure for $YBa_2Fe_3O_8$ (Ref. 7).

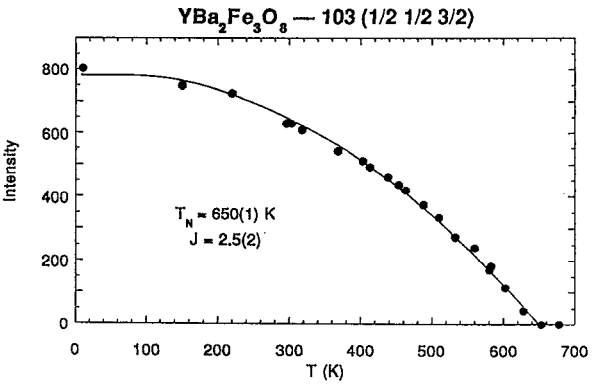


FIG. 3. Temperature dependence of the intensity of the magnetic reflection.

Experimentally we can recognize the magnetic scattering by several characteristics. First, it should be temperature dependent, and the Bragg peaks will vanish above the ordering temperature. Figure 3 shows the temperature dependence of the intensity of the peak at 19.5°, which clearly reveals a phase transition at 650 K. A second characteristic is that the magnetic intensities become weak at high scattering angles (not shown), as $f(\tau)$ typically falls off strongly with increasing angle. A third, more elegant, technique is to use polarized neutrons. The polarization technique can be used at any temperature, and for any material regardless of whether or not it has a crystallographic distortion (e.g., via magnetoelastic interactions) associated with the magnetic transition. It is more involved and time-consuming experimentally, but yields an unambiguous identification and separation of magnetic and nuclear Bragg peaks.

The polarization analysis technique as applied to this problem is in principle straightforward.[8] Nuclear coherent Bragg scattering never causes a reversal, or spin-flip, of the neutron spin direction upon scattering. Thus the nuclear peaks will only be seen in the non-spin-flip [denoted by $(++)$] scattering geometry. The magnetic cross sections depend on the relative orientation of the neutron polarization $\mathbf{P}$ and the reciprocal lattice vector transfer $\tau$. In the configuration where $\mathbf{P}\perp\tau$, half the magnetic Bragg scattering involves a reversal of the neutron spin [denoted by the $(-+)$ configuration], and half does not. Thus for the case of a purely magnetic reflection the spin-flip $(-+)$ and non-spin-flip $(++)$ intensities should be equal in intensity. For the case where $\mathbf{P}\|\tau$, all the magnetic scattering is spin-flip. Hence for a magnetic Bragg peak the spin-flip scattering should be twice as strong as for the $\mathbf{P}\perp\tau$ configuration, while ideally no non-spin-flip scattering will be observed. Figure 4 shows the polarized beam results for the same two peaks, at scattering angles (for this wavelength) of 30° and 35°; these correspond to the peaks at 19.5° and 23° in Fig. 1. The top section of the figure shows the data for the $\mathbf{P}\perp\tau$ configuration. The peak at 30° has the identical intensity for both spin-flip and non-spin-flip scattering, and hence we conclude that this scattering is purely magnetic in origin as inferred from Fig. 3. The peak at 35°, on the other hand, has strong intensity for $(++)$, while the intensity for $(-+)$ is smaller by a factor of 1/11, the instrumental flipping ratio. Hence this peak is a pure



Downloaded 10 Nov 2003 to 129.6.121.15. Redistribution subject to AIP license or copyright, see http://ojps.aip.org/japo/japcr.jsp

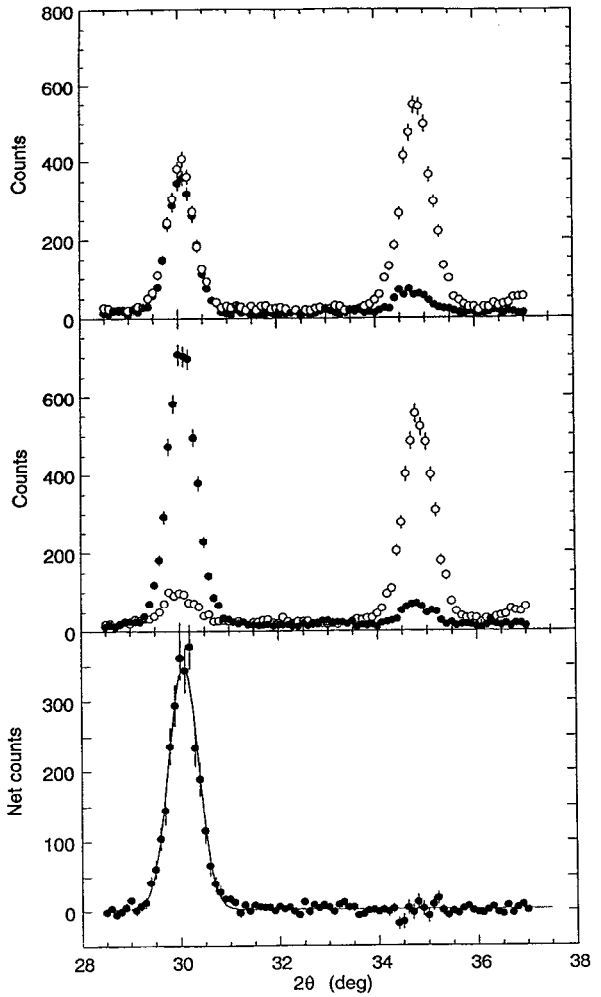


FIG. 4. Polarized neutron scattering. The top portion of the figure is for $\mathbf{P}\perp\boldsymbol{\tau}$, where the open circles ○ show the non-spin-flip scattering and the filled circles ● are the observed scattering in the spin-flip configuration. The low angle peak has equal intensity for both cross sections, and thus is identified as a pure magnetic reflection, while the ratio of the (++) to (−+) scattering for the high angle peak is 11, the instrumental flipping ratio. Hence this is a pure nuclear reflection. The center portion of the figure is for $\mathbf{P}\parallel\boldsymbol{\tau}$, and the bottom portion is the subtraction of the $\mathbf{P}\parallel\boldsymbol{\tau}$ spin-flip from the data for $\mathbf{P}\perp\boldsymbol{\tau}$. Note that in the subtraction procedure all background and nuclear cross sections cancel, isolating the magnetic scattering (Ref. 7).

nuclear reflection. The center row shows the same peaks for the $\mathbf{P}\parallel\boldsymbol{\tau}$ configuration, while the bottom row shows the subtraction of the $\mathbf{P}\perp\boldsymbol{\tau}$ spin-flip scattering from the $\mathbf{P}\parallel\boldsymbol{\tau}$ spin-flip scattering. In this subtraction procedure instrumental background, as well as all nuclear scattering cross sections, cancel, isolating the magnetic scattering. We see that there is magnetic intensity only for the low angle position, while no intensity survives the subtraction at the 35° peak position. These data unambiguously establish that the 30° peak is purely magnetic, while the 35° peak is purely nuclear. This simple example demonstrates how the technique works; obviously it would play a much more critical role in cases where it is not clear from other means what is the origin of the peaks, such as in regimes where the magnetic and nuclear

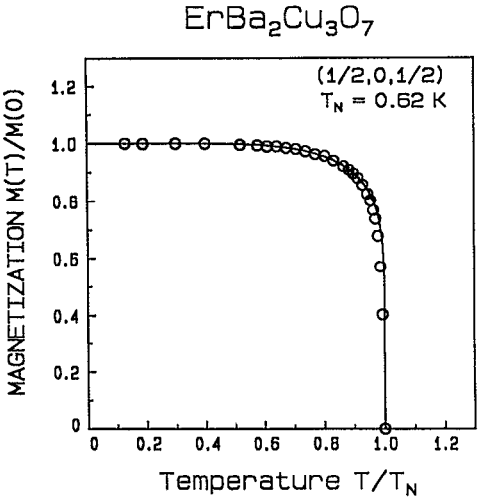


FIG. 5. Temperature dependence of the sublattice magnetization for the Er spins in superconducting $ErBa_2Cu_3O_7$, measured on a single crystal weighing 31 mg. The solid curve is Onsager's exact theory for the two-dimensional, $S=\frac{1}{2}$, Ising model (Ref. 9).

peaks overlap,[7] or in situations where the magnetic transition is accompanied by a structural distortion.

Another example of magnetic diffraction[9] is shown in Fig. 5. Here we show the intensity of a Bragg peak as a function of temperature for the Er ordering in $ErBa_2Cu_3O_7$. The magnetic interactions in this material are highly anisotropic, and this system turns out to be an ideal two-dimensional (planar) Ising antiferromagnet; the solid curve is Onsager's exact solution to the $S=\frac{1}{2}$, 2-D Ising model, and we see that it provides an excellent representation of the experimental data.

A final diffraction example is shown in Fig. 6, where the data for a series of molecular beam epitaxy $Fe_3O_4$/NiO superlattices are shown.[10] These scans are along the growth direction ($Q_z$), and we see the (222) fundamental peak (to-

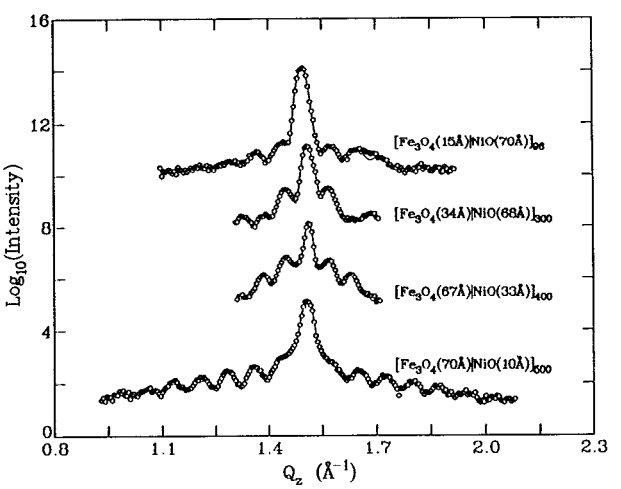


FIG. 6. Observed scattering from a series of $Fe_3O_4$/NiO multilayers with different layer depths and total thickness. The satellites observed about the fundamental (222) reflection in the center originate from both nuclear and magnetic scattering. The typical weight of these samples is 1 mg (Ref. 10).



Downloaded 10 Nov 2003 to 129.6.121.15. Redistribution subject to AIP license or copyright, see http://ojps.aip.org/japo/japcr.jsp

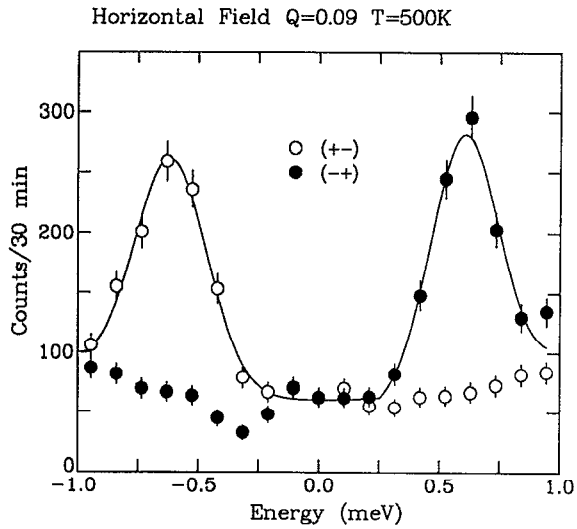


FIG. 7. Spin-flip scattering observed for the amorphous Invar $Fe_{86}B_{14}$ system in the $\hat{P}\|\mathbf{Q}$ configuration. Spin waves are observed for neutron energy gain ($E<0$) in the ($+-$) cross section, and for neutron energy loss ($E>0$) in the ($-+$) configuration (Ref. 11).

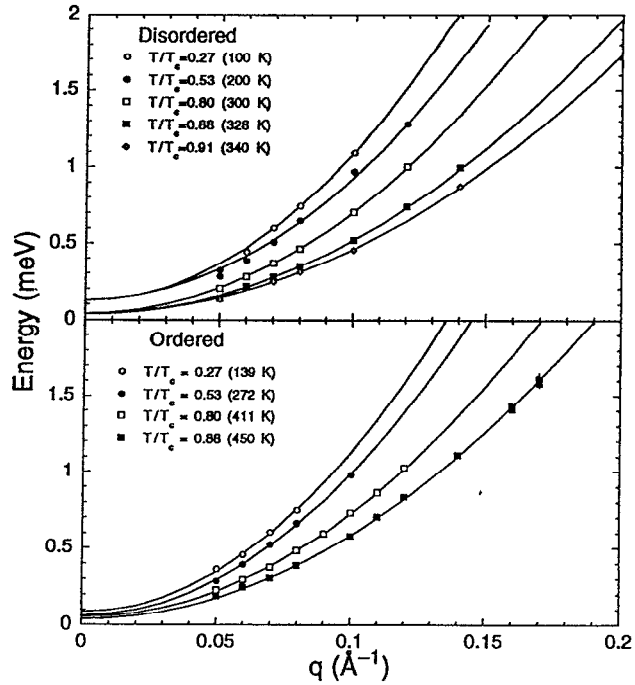


FIG. 8. Measured spin wave dispersion relations for chemically disordered (top) and ordered (bottom) $Fe_3Pt$ (Ref. 12).

gether with a peak from the MgO substrate) along with a series of satellite peaks on either side. The satellite peaks have both nuclear and magnetic contributions, and from such data the crystallographic and magnetic coherence lengths both in and between the layers can be followed as a function of temperature, field, thickness, etc.

It is interesting to compare the type and quality of data that are represented by these three examples. The powder diffraction technique is quite straightforward, both to obtain and analyze data. In this case typical sample sizes are ~5 g, and important and detailed information can be readily obtained with such sample sizes in a few hours of spectrometer time. The temperature dependence of the order parameter in $ErBa_2Cu_3O_7$, on the other hand, was obtained on a single crystal weighing only 31 mg. Note that the quality of the data is much better than for the powder sample even though the sample is more than two orders-of-magnitude smaller. The final example was for $Fe_3O_4$/NiO multilayers, where the weight of the superlattices that contributes to the scattering ranges from 0.3–1.5 mg. Thus it is clear that interesting and successful diffraction experiments can be carried out on quite small samples.

## III. MAGNETIC EXCITATIONS

Inelastic neutron scattering plays a unique role in determining the magnetic excitation spectra in magnetic systems, as it is the only probe that can directly measure the complete magnetic excitation spectrum. Typical examples are spin wave dispersion relations, critical fluctuations, crystal field excitations, and moment/valence fluctuations. Here we give an example of some spin wave measurements utilizing inelastic polarized beam techniques, which is a technique that is finding increasing use. In the long wavelength (small $q$) regime the spin wave dispersion relation for an isotropic ferromagnet is given by $E_{sw}=D(T)q^2$, where $D$ is the spin wave "stiffness" constant. The general form of the spin wave dispersion relation is the same for all isotropic ferromagnets, while the numerical value of $D$ depends on the details of the magnetic interactions and the nature of the magnetism. One example of a prototypical isotropic ferromagnet is amorphous $Fe_{86}B_{14}$. Figure 7 shows an example of polarized beam inelastic neutron scattering data taken on this system.[11] To understand these data we note that spin wave scattering, represented in the Hamiltonian by the raising and lowering operators $S^{\pm}=S^x\pm iS^y$, causes a reversal of the neutron spin. These spin-flip cross sections are denoted by ($+-$) and ($-+$). If the neutron polarization $\hat{P}$ is parallel to the momentum transfer $\mathbf{Q}$, $\hat{P}\|\mathbf{Q}$, then we should be able to create a spin wave only in the ($-+$) configuration, or destroy a spin wave only in the ($+-$). This is precisely what we see in the data; for the ($-+$) configuration the spin waves can only be observed for neutron energy loss scattering ($E>0$), while for the ($+-$) configuration spin waves can only be observed in neutron energy gain ($E<0$). We remark that the cross sections for inelastic scattering are typically several orders-of-magnitude smaller than for elastic Bragg scattering, and thus large samples are required for these types of measurements; the sample in this case weighed ~10 g.

Data like these can be used to measure the renormalization of the spin waves as a function of temperature, as well as determine the lifetimes as a function of wave vector and temperature. An example for the crystalline Invar-type ferromagnet $Fe_3Pt$ is shown[12] in Fig. 8. Here we have determined the wave vector dependence of the dispersion relation at a series of temperatures, both for the chemically ordered and disordered single crystals. These measurements can then be compared with theory as well as other experimental observa-



Downloaded 10 Nov 2003 to 129.6.121.15. Redistribution subject to AIP license or copyright, see http://ojps.aip.org/japo/japcr.jsp

TABLE I. Neutron scattering spectrometers available for materials research in magnetism at the various neutron scattering centers in the U.S. Brookhaven National Laboratory (BNL) and the National Institute of Standards and Technology (NIST) operate heavy water reactors, while Oak Ridge National Laboratory (ORNL) and the University of Missouri (UM) operate light water reactors. The neutron sources at Argonne National Laboratory (ANL) and Los Alamos National Laboratory (LANL) are pulsed spallation facilities. NA=not applicable; C signifies under construction/development. At ORNL some spectrometers share a beam port and are therefore only available part time.

| Spectrometer | ANL | BNL | LANL | NIST | ORNL | UM |
|---|---|---|---|---|---|---|
| SANS | 1+1*C* | 2 | 1 | 3 | 2 | 1*C* |
| Triple axis | NA | 5 | NA | 5+1*C* | 4 | 1 |
| Inelastic TOF | 4 | 0 | 2 | 1+1*C* | 1 | 0 |
| High res. powder | 2 | 1 | 1 | 1 | 1 | 1 |
| High intensity powder | 1 | 1+1*C* | 1 | 0 | 1 | 0 |
| Diffractometer | 2 | 3+1*C* | 1 | 1*C* | 2 | 2 |
| Spin echo | 0 | 0 | 0 | 1*C* | 0 | 0 |
| Backscattering | 0 | 0 | 1*C* | 1*C* | 0 | 0 |
| Reflectometer | 2 | 1 | 1 | 2+1*C* | 1 | 1 |
| User contact | T. Worlton | R. Greenberg | M. DiStravolo | W. Kamitakahara | R. Nicklow | J. Rhyne[a] |

[a]UM has no formal user program, and research there is accommodated on a collaborative basis only.

tions (such as magnetization measurements) which are controlled by such spin wave excitations.

## IV. NEUTRON FACILITIES

The neutron scattering facilities available in the U.S. are shown in Table I. The National Laboratories all have ongoing user programs to acquire beam time, while the research at the University of Missouri reactor is done on a collaborative basis only. Brookhaven National Laboratory, Oak Ridge National Laboratory, and the National Institute of Standards and Technology operate research reactors, which provide steady beams of thermal, and in the case of NIST and BNL, cold neutrons. The NIST cold source supports a guide hall facility which can accommodate 15 or more instrumental stations when completed; it is the only project presently under construction. Argonne National Laboratory and Los Alamos National Laboratory have pulsed spallation neutron sources. This technique for producing neutrons in general is complementary to steady-state reactor sources, and the pulsed nature of the sources means that all instruments operate on the time-of-flight principle. The person to contact for more information about these facilities is provided at the bottom of the table.

Neutrons provide a unique tool not only for magnetism, but for broad areas of materials science, physics, chemistry, biology, and nuclear medicine. The reactors that are presently in use have already been operating for a quarter of a century, and there is a detailed plan to build a new research reactor, the advanced neutron source, to replace some of these facilities. The ANS would provide an order-of-magnitude more raw flux, and would also allow dramatic improvements in beam optics for many instruments; a great deal has been learned (and invented) in the last 25 years about how to optimize neutron scattering instrumentation. If authorized for construction next year, the ANS would come on line early next decade, and would allow the U.S. to recapture the lead in the neutron scattering field. There are also plans to develop a design for a new, higher intensity spallation source. If these new facilities become a reality, then neutron scattering in the U.S. will continue to play a vital role in magnetism in particular and condensed matter physics in general, well into the next century.

## ACKNOWLEDGMENTS

I would like to thank my NIST colleagues, J. A. Borchers, N. Rosov, Q. Huang, and P. Gehring, for their assistance. I would also like to thank J. D. Axe, R. M. Nicklow, J. J. Rhyne, R. A. Robinson, and T. Worlton for the information they provided.

[1] S. W. Lovesey, *Theory of Neutron Scattering from Condensed Matter* (Oxford, New York, 1984), Vol. 2.
[2] E. Balcar and S. W. Lovesey, *Theory of Magnetic Neutron and Photon Scattering* (Oxford, New York, 1989).
[3] G. E. Bacon, *Neutron Diffraction* (Oxford U.P., Oxford, 1975), 3rd ed.
[4] W. Gavin Williams, *Polarized Neutrons* (Oxford, New York, 1988).
[5] G. L. Squires, *Thermal Neutron Scattering* (Cambridge, New York, 1978).
[6] *Methods of Experimental Physics: Neutron Scattering*, edited by D. L. Price and K. Sköld (Academic, Orlando, 1987), Parts C, A, and B.
[7] Q. Huang, P. Karen, V. L. Karen, A. Kjekshus, J. W. Lynn, A. D. Mighell, N. Rosov, and A. Santoro, Phys. Rev. B **45**, 9611 (1992).
[8] R. M. Moon, T. Riste, and W. C. Koehler, Phys. Rev. **181**, 920 (1969).
[9] J. W. Lynn, T. W. Clinton, W-H. Li, R. W. Erwin, J. Z. Liu, K. Vandervoort, and R. N. Shelton, Phys. Rev. Lett. **63**, 2606 (1989).
[10] J. A. Borchers, R. W. Erwin, S. D. Berry, D. M. Lind, E. Lochner, K. A. Shaw, and D. Hilton, Appl. Phys. Lett. **64**, 381 (1994).
[11] J. W. Lynn, N. Rosov, and G. Fish, J. Appl. Phys. **73**, 5369 (1993).
[12] N. Rosov, J. W. Lynn, J. Kästner, E. F. Wassermann, T. Chattopadhyay, and H. Bach (these proceedings).



Downloaded 10 Nov 2003 to 129.6.121.15. Redistribution subject to AIP license or copyright, see http://ojps.aip.org/japo/japcr.jsp